Urban Climate 53 (2024) 101811

Contents lists available at ScienceDirect

Urban Climate

journal homepage: www.elsevier.com/locate/uclim

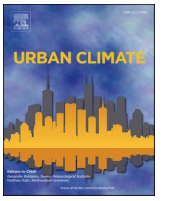

Evaluation of surface air temperature in the HARMONIE-AROME weather model during a heatwave in the coastal city of Turku, Finland

Juuso Suomi [a,*], Olli Saranko [b], Antti-Ilari Partanen [c], Carl Fortelius [b], Carlos Gonzales-Inca [a], Jukka Käyhkö [a]

[a] Section of Geography, Department of Geography and Geology, University of Turku, Turku FI-20014, TURUN YLIOPISTO, Finland
[b] Meteorological Research, Finnish Meteorological Institute, Helsinki, P.O. BOX 503, FI-00101, HELSINKI, Finland
[c] Climate System Research, Finnish Meteorological Institute, Helsinki FI-00101, P.O. BOX 503, Finland

ARTICLE INFO

Keywords:
Numerical weather prediction model
HARMONIE-AROME
Temperature modelling
Urban heat island
Land cover
Heatwave

ABSTRACT

Performance of meso-scale numerical weather prediction model HARMONIE-AROME was assessed for a summer-time heatwave in a high-latitude coastal city of Turku in SW Finland. Representativeness of the model's ECOCLIMAP-SG based physiographic land cover specification with a resolution of 750 m was assessed against the 20 m resolution CORINE Land Cover (CLC) dataset. Moreover, the modelled 2 m air temperatures were compared with temperature observations recorded at 74 sites of the local climate observation network. Correlation analysis between the model's physiographic data (PGD) and CLC shows a statistically significant ($p \leq 0.01$) match between the datasets in 76% of the land cover types, indicating mainly a good representativeness of the HARMONIE-AROME's land cover parameterization in the study area. The cases of mismatch are mostly related to the differences in ECOCLIMAP-SG and CLC classification principles and/or resolution, and thus can not be considered to indicate poor representativeness of the ECOCLIMAP-SG classification in the area. The HARMONIE-AROME modelled temperatures were on average slightly higher than the observed temperatures, and the difference was largest for daily minimum temperatures. Heterogeneity of land cover and topography inside a 750 m grid cell was related to larger difference between the modelled and observed temperature.

1. Introduction

Urban areas form their own specific type of local climate. Probably the most studied and best recognizable phenomenon of urban climate is the urban heat island (UHI), which refers to the warmness of the urban areas compared to their rural surroundings. The UHI results from high heat storage capacity and good thermal conductivity of typical urban construction materials, anthropogenic heat release from buildings, traffic, industry and human metabolism, and lower evapotranspiration compared to the surrounding rural areas (Landsberg, 1981; Oke, 1987; Bahi et al., 2020). In addition to the impact of the city, temperature can vary locally due to the impacts of other environmental factors, such as topography and water bodies. This variation has city-specific differences, and within a certain

* Corresponding author.
E-mail addresses: juuso.suomi@utu.fi (J. Suomi), olli.saranko@fmi.fi (O. Saranko), Antti-Ilari.Partanen@fmi.fi (A.-I. Partanen), carl.fortelius@fmi.fi (C. Fortelius), cagoin@utu.fi (C. Gonzales-Inca), jukka.kayhko@utu.fi (J. Käyhkö).

https://doi.org/10.1016/j.uclim.2024.101811
Received 14 April 2022; Received in revised form 5 October 2023; Accepted 16 January 2024
Available online 29 January 2024

city, the variation has often diurnally and seasonally varying characteristics (Suomi and Käyhkö, 2012). In spring, autumn and winter the UHI is in high latitude regions often considered a neutral or slightly positive phenomenon due to the longer growth season and savings in heating costs (Waffle et al., 2017; Roxon et al., 2020), but in summer, the UHI for its part increases the heat stress and related health risks during the heatwaves (Ruuhela et al., 2017; 2021). Even if there is no uniform opinion on whether the UHI intensity will decrease on increase as a consequence of climate change (Wilby, 2007; Oleson et al., 2011; Scott et al., 2018; Fenner et al., 2019), the general warming trend will increase the relevance of heat-related health aspects in high-latitudes in the future.

Knowledge on local temperature variability can be utilised e.g. in urban planning (Bhargava et al., 2017; Elliott et al., 2020). To be appropriate, planning should be based on spatially continuous and accurate temperature information. This often remains a challenge, as in many cities temperatures are measured in one or few sites only. To tackle the challenge, various temperature modelling approaches have been applied (Mirzaei, 2015; Hollósi et al., 2021; MacLachlan et al., 2021). In scientific literature, UHI modelling has been grouped in different ways. Atkinson (2003) divides the UHI modelling to three approaches: hardware modelling, physical modelling using the surface energy budget equation and dynamic numerical modelling that, in addition to the surface forcing functions, often includes the advective component of the climate. Mirzaei (2015) divides the UHI models based on their scales to building-scale models, micro-scale models and city-scale models. During the recent decades, novel methods to model UHI have been applied, but there still remains a challenge to precisely embed the complex urban infrastructure and relevant physical processes in the models (Imran et al., 2021).

As a consequence of increasing amount of open access remotely sensed (RS) data, the surface urban heat island (SUHI) that is determined by differences in surface temperatures, has become rather popular branch of the UHI research since the end of the 20th century (Voogt and Oke, 2003; Shi et al., 2021). Better availability of RS and other Geographic Information System (GIS) data has enriched also the UHI research that is based on air temperature. GIS based modelling methods have proven to be rather cost-effective in determining the intensity and spatial characteristics of UHI (Szymanowski and Kryza, 2009; Nakata-Osaki et al., 2018; Burger et al., 2021). Beyond the actual GIS based modelling, better availability of open access GIS datasets has broadened the possibilities to assess and develop models that as such can be considered to represent some other realm than GIS based modelling. Of the multiple modelling approaches, our focus in this study is on numerical weather prediction modelling.

Numerical weather modelling simulates complex interactions between land surface characteristics and atmosphere over wide ranges. Land use / land cover data are an essential input for model parameterization, as land cover composition directly influences the energy and water fluxes at the soil-atmosphere interface (Sertel et al., 2010). The use of high-quality land cover data has proven to improve the modelling accuracy (Kirthiga and Patel, 2018; López-Espinoza et al., 2020). However, the use of high-resolution land cover data has been limited in numerical simulation due to high computational demand and challenges in the availability of appropriate datasets. Even if the proper high-resolution datasets would be available, the computational demands often result in that rather coarse resolution land cover data used in numerical modelling. The resolution may be a challenge especially in urban environments, in which the temperatures can vary remarkably even in a short distance (Klysik and Fortuniak, 1999; Saaroni et al., 2000). Even if land cover data would be appropriate, successful parametrisation and quantification of urban surface parameters has been challenging in many earlier studies (Samsonov and Varentsov, 2020).

For a fine-scale urban weather mapping, several statistical downscaling methods have been evaluated (DuchÊne et al., 2020; Le Roy et al., 2021; Serifi et al., 2021); most of them are based on establishing a relationship between regional numerical weather forecasts and land cover and urban morphological properties (DuchÊne et al., 2020), and consequently, a good understanding of the effect of land cover details on numerical model output is crucial. In this study, we will focus on the performance of numerical weather prediction model HARMONIE-AROME (Bengtsson et al., 2017) in a coastal high-latitude city during a summer-time heatwave, as these kind of weather conditions are most relevant from a health perspective already in current climate (Kollanus et al., 2021; Ruuhela et al., 2021), and even more so in the future. The ECOCLIMAP-SG based land use / land cover specification of HARMONIE-AROME numerical weather prediction model at 750 m X 750 m resolution is compared to the 20 m × 20 m resolution CORINE Land Cover (CLC) dataset in the city of Turku area and its surroundings in the south-western Finland. Additionally, HARMONIE-AROME modelled air temperatures of 750 m × 750 m spatial resolution are analyzed against the observed air temperatures of 74 observation sites at the same area. The objectives of this study are to:

1) Assess the spatial correspondence of the land use / land cover (LULC) specification of HARMONIE-AROME model and high-resolution LULC dataset and thereby find out how the observed correspondence might explain errors in the model output especially in the urban study area.
2) Find out how much do the air temperatures modelled by HARMONIE-AROME differ from the observed air temperatures recorded by a dense urban climate observation network.
3) Unravel the spatial pattern of the differences and the role of land surface factors (land use, urban morphology, topography, water bodies) in explaining the differences between the modelled and observed temperatures.
4) Find out which kind of diurnal and weather-specific variation do the differences have and which factors might explain that variation.

2. Materials and methods

2.1. Study area

Our study area consists of a middle-size (195,000 inhabitants) coastal city of Turku and parts of its neighbouring municipalities.

The total extent of the study area is 113 km in east-west dimension and 76 km in north-south dimension. Turku is located in south-western Finland (city centre: 60°27′N, 22°16′E) at the mouth of river Aura (Fig. 1). Relatively large islands immediately off-shore the city centre and wide archipelago further to the south-west of the city make the climate of Turku as a combination of coastal and inland types. Location and movements of large weather systems determine whether continental or marine characteristics dominate (Alalammi, 1987).

In Köppen's climate classification, Turku belongs to the hemiboreal and humid Dfb class together with Baltic countries, eastern Europe, southern parts of Scandinavian Peninsula, Great Lakes region and mid-latitudes of western Asia. For the period 1991–2020, the annual average temperature at Turku Airport, approximately 7 km to the north of the city centre, was 5.8 °C (Jokinen et al., 2021). Coldest month was February with average temperature of −4.5 °C, average daily minimum temperature of −7.1 °C and average daily maximum temperature of −1.2 °C. Warmest month was July, when the respective temperatures were 17.5 °C, 12.5 °C and 22.6 °C. Highest measured temperature during 1991–2020 was 33.0 °C, observed in July 2018, whereas the coldest temperature was −28.2 °C, observed in January 2013. Mean annual rainfall in the study area was 684 mm. The driest month was April (32 mm), whereas the wettest one was July (74 mm). Length of permanent snow cover period increases from archipelago towards the inland, and is in the surroundings of the Turku city centre approximately three months, starting typically at the turn of the year (SYKE et al., 2020). Average annual wind speed in the area was 3.4 m/s. The average wind speed was strongest in December (3.7 m/s), and weakest (3.1 m/s) in July, August and September. Dominant wind direction (16%) was southeast, whereas least (8%) blew from north and northeast.

The street orientation in the grid plan area of the city centre is from SW to NE and from SE to NW. The extent of the rectangular grid plan is approximately 1.5 km in SE-NW dimension and 4 km in SW-NE dimension. The grid plan area mostly consists of 6–8 storey high blocks of flats, and interleaving parks. The commercial activities are concentrated in the surroundings of the market place that is

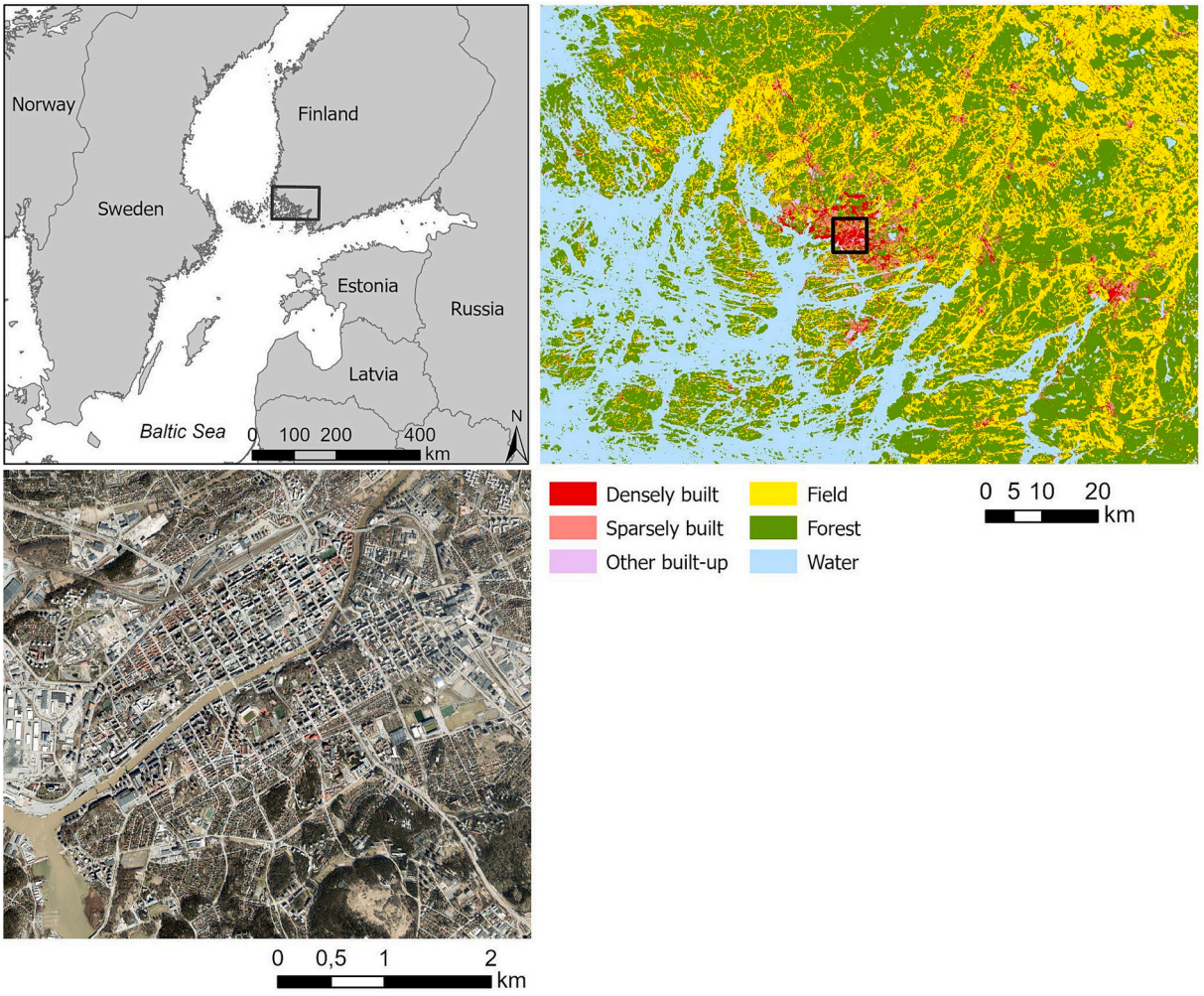

Fig. 1. The study area in a broader geographical context (upper left), land cover in the study area (upper right) and aerial image of the Turku city centre. The land cover map is reclassified from the CLC2018 dataset. For detailed information on the original CLC2018 classification, see Appendix A. The aerial image is an orthophoto produced by the National Land Survey of Finland in 2020.

located in the middle of the grid plan area. The Aura River flows from NE to the SW in the middle of the grid plan. The width of the river in the city centre varies between 50 m and 100 m. There are a couple of 30–50 m high hills in the grid plan area, but for most part it consists of relatively flat terrain with elevation of 5–10 m above the sea level. Beyond the grid plan area land cover is a mosaic of built-up areas, forests and fields (Turku, 2021).

2.2. TURCLIM temperature data

Temperature observations have been collected as part of the Turku Urban Climate Research Project TURCLIM of the Geography Division at the University of Turku. The TURCLIM observation network currently consists of altogether 75 Onset Hobo Pro v2 U23–001 temperature and relative humidity data loggers. The loggers are placed inside Onset RS1 radiation shields on poles at 3 m elevation above the ground. The elevation differs from the standard 2 m elevation in order to minimise the risk of vandalism. The observation interval is 30 min. According to the manufacturer, the accuracy of the instrument is ±0.2 °C at 0–70 °C, and ± 0.25 °C at −40–0 °C, while the resolution is 0.04 °C. In this study, we use temperature observations of 74 sites (Fig. 2; Appendix B).

2.3. ECOCLIMAP-SG land cover data

In HARMONIE-AROME cycle 43 h used here, ECOCLIMAP Second Generation (ECO-SG) is the base of land cover physiography. (Samuelsson et al., 2020) In ECO-SG, the surface land use is divided into 33 different cover types. Each type belongs to one (and only one) of the following four tiles: sea, inland water bodies, nature and urban. The ten urban cover types in ECO-SG represent the ten Local Climate Zones (Stewart and Oke, 2012; CNRM, 2018).

ECO-SG dataset is based on different data sources. In Europe, the urban covers are based on CORINE Land Cover dataset from 2012 and on data from Global Human Settlement Layer (GHSL, 2022). For vegetation and water bodies, several data sources were used based on the location (CNRM, 2018). These datasets were used to create a 300 m-resolution grid with pure typing, meaning that each grid cell contains only one cover type. (CNRM, 2018).

When the HARMONIE-AROME model experiment is started, it creates a dataset to describe the physiography of the domain. The resolution of the dataset is the same as the experiment's and it is based on the ECO-SG dataset. This new dataset, called the PGD (physiographic data), doesn't have a pure typing like ECO-SG, as the covers are now presented with a percentage. The PGD is used when the model calculates interactions between the atmosphere and the surface.

2.4. CORINE Land Cover (CLC) data

CORINE is a pan-European land cover classification coordinated by the European Environmental Agency and produced in the context of the Copernicus Land Monitoring Service. CORINE has a long history; a first land cover inventory was initiated in 1985, and the first dataset was published in 1990 (Copernicus, 2021). It is widely used for different types of studies including climate (Kim et al.,

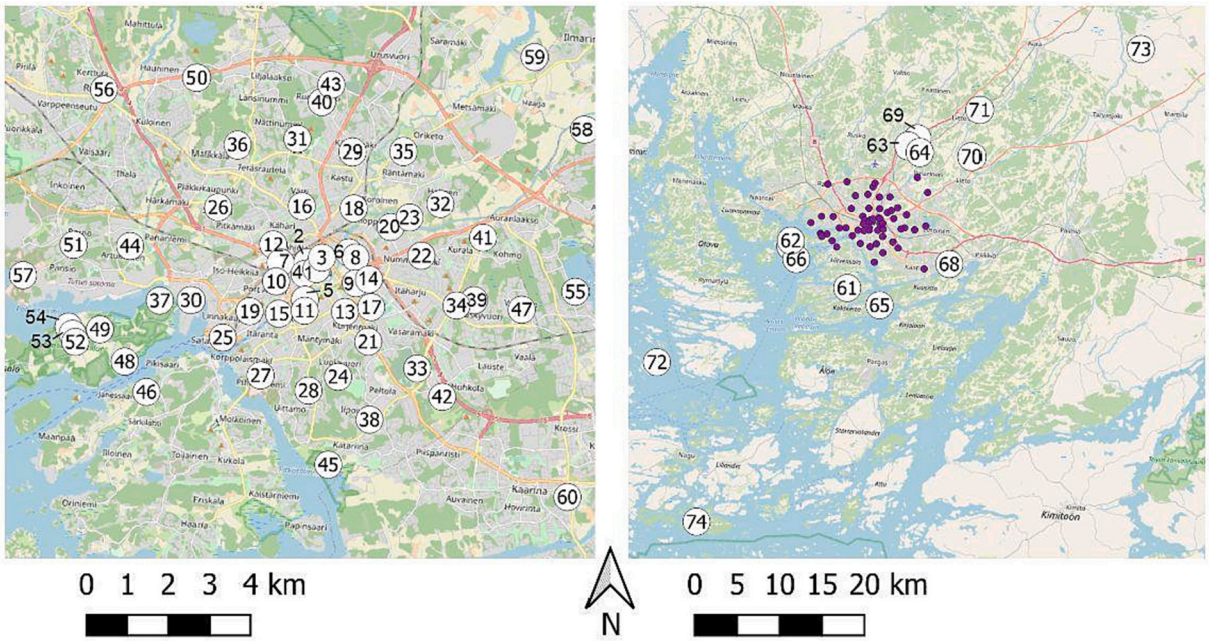

Fig. 2. TURCLIM observation sites used in the study. The observation site numbers correspond with the observation site numbers in the Appendix B. Background map: OpenStreetMap.

2013; Törmä et al., 2015; Emery et al., 2021; Reinhart et al., 2021; de Bode et al., 2023) and other fields of science (Rusu et al., 2020; Mingarro and Lobo, 2023). In this study, we use the CLC2018 dataset that was published in 2018. CLC2018 in Finland has an overall accuracy of 92%, and it shows over 95% accuracy for most of the land cover classes (Moiret-Guigand, 2021). Good accuracy has been detected also in other high-latitude areas (Aune-Lundberg and Strand, 2021). The dataset has 4 classification levels. The raster version applied in this study represents the level 4 classification that is the most detailed one having altogether 49 classes. The spatial resolution is 20 m (SYKE, 2021; For map view and table of the classes, see Appendix A).

2.5. HARMONIE-AROME model

HARMONIE-AROME (Bengtsson et al., 2017), is a high-resolution model used for short-range weather forecasting by 10 European meteorological services including the Finnish. The model is developed in the international ACCORD consortium formed by 26 services in Europe and in North Africa (ACCORD, 2022). HARMONIE-AROME is a convection-permitting limited area model using non-hydrostatic dynamics. Sub-grid scale parameterized physical processes in the atmosphere include cloud microphysics and precipitation, radiative transfer, turbulence and shallow convection. Processes at the lower boundary are treated in the frame of an autonomous surface and soil module (SURFEX, Masson et al., 2013).

The heterogeneity of the surface is addressed by using a so-called tiling approach, where several of the surface types (sea, inland water, nature, and urban) may be present in a given grid cell (e.g. Masson et al., 2013). All the surface types, or tiles, within a given grid cell experience the same atmospheric conditions, "forcing", but react individually, according to their respective physical properties. The response of individual tiles, in the form of fluxes of energy, moisture, and momentum, are aggregated into a representative average for the grid cell, which is then allowed to influence the atmosphere. In SURFEX, the physical properties of the tiles of vegetated and built-up represent aggregates of patches of different vegetation types or local climate zones present within the tile. Nature and urban tiles of ECO-SG are handled by ISBA (Noilhan and Planton, 1989) and TEB (Masson, 2000) models, respectively. Further details are provided by Bengtsson et al. (2017) and references therein.

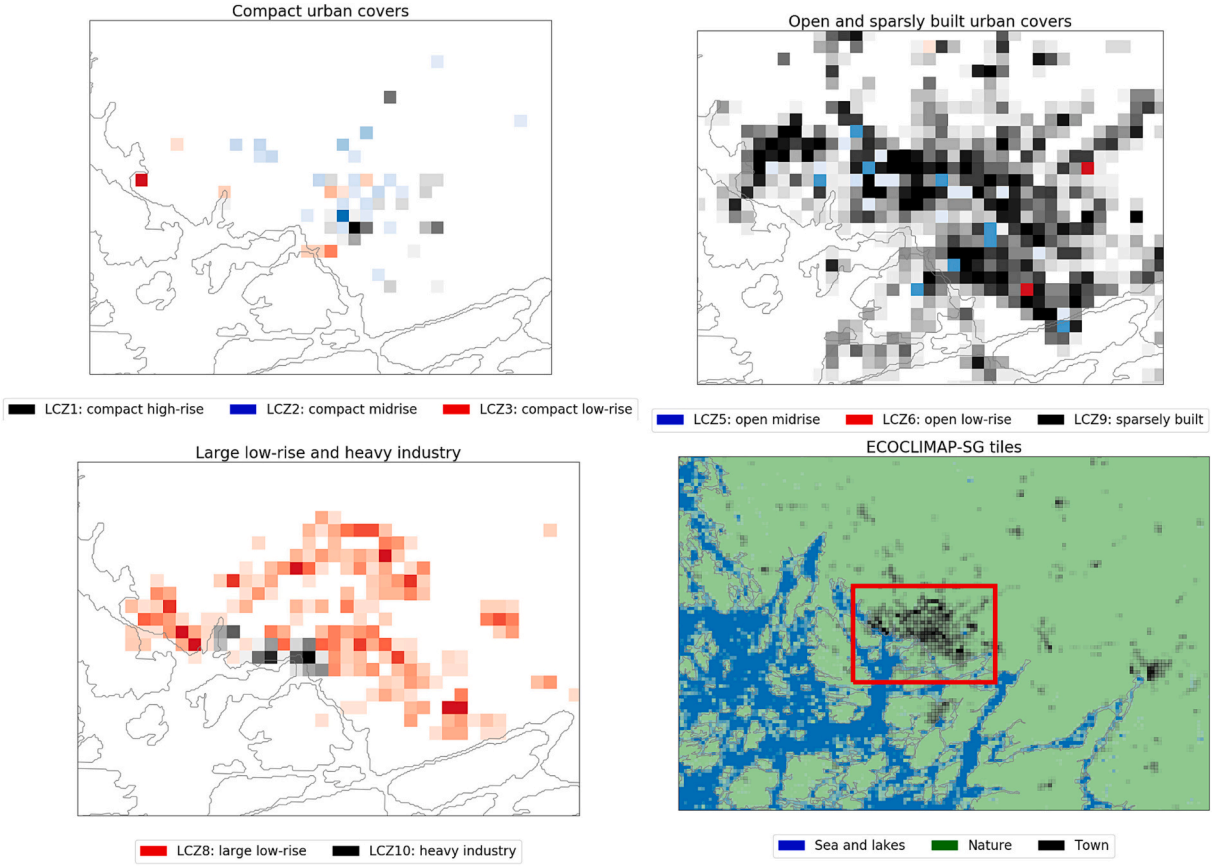

Fig. 3. The urban cover types and ECOCLIMAP-SG tiles of the HARMONIE-AROME experiment are shown in the four panels. Top left: LCZ1 (black), LCZ2 (blue) and LCZ3 (red); top right: LCZ5 (blue), LCZ6 (red) and LCZ9 (black); bottom left: LCZ8 (red) and LCZ10 (black); bottom right: sea and water tiles (blue), nature tiles (green) and town tiles (black).The zoomed map of the city center of Turku presented in the three cover-maps is indicated with the red rectangle in the tile-map. (For interpretation of the references to colour in this figure legend, the reader is referred to the web version of this article.)

TEB model follows the canyon approach, where the urban energy budget is calculated in three separate surfaces: roofs, walls and roads. TEB takes into account several physical processes which include: 1) shortwave and longwave trapping effect of the canyon geometry; 2) anthropogenic sensible heat flux; 3) water and snow interception by the roads and roofs; 4) heat conduction and storage in buildings and roads; 5) interactions between canyon air and built surfaces. (Masson et al., 2013).

ISBA is used to model the biophysical processes of soil and vegetation related variables, and their interactions with the atmosphere. For further details regarding the processes and interactions available in the model, see for example Masson et al. (2013). The modelling process is constantly updated to match the growing need to represent these interactions more accurately.

The present study uses version cy43h2 of HARMONIE-AROME with a horizontal grid spacing of 750 m and 65 levels in the vertical. The lowest model level is at 12 m above the surface, and the model top at 10 hPa. The computational domain is centered over Southern Finland (center point at 60.83°N, 23.68°E), with dimensions of 800 by 720 grid cells. Surface characteristics given in ECO-SG (CNRM, 2018) were used, but near the coasts some sea areas erroneously classified as lakes were corrected based on local data. HARMONIE-AROME was nested into operational analyses of the ECMWF (European Centre for Medium Range Weather Forecasts), and run in forecast cycles with surface and soil variables analyzed every six hours based on observed 2 m temperature and humidity. Forecasts of 24 h with an output frequency of one hour were initiated every day at 00 and 12 UTC, while only 6-hourly forecasts were computed at 06 and 18 UTC.

2.6. *Evaluation of ECOCLIMAP-SG based physiographic data in the study area*

The validity of the ECO-SG based physiographic data (PGD) as a describer of climatically relevant characteristics of the study area was assessed by calculating Pearson's correlation coefficients between the areas of a certain land cover type that is represented in the PGD and CORINE classifications inside each 750 m grid cell, which is the spatial resolution of this HARMONIE-AROME experiment and the resolution of the PGD. Before the correlation analysis, a corresponding CORINE class was determined for each ECO-SG cover type that is represented in the study area. Apart from single classes, also combinations of classes were tested, when considered appropriate. For examples of urban cover types and ECO-SG tiles of the HARMONIE-AROME experiment, see Fig. 3.

2.7. *Temperature modelling and comparison with the observed temperatures*

The HARMONIE-AROME experiment was conducted for the period 1.7.-5.8.2018. Before the actual experiment, the period 15.-30.6.2018 was run as a start up. In this study the focus was on the period 25.-31.7.2018, as there was an unusual heat-wave on that time in Finland. Heat-waves are relevant from a health perspective, and their relevance will further increase as a consequence of climate change. The instantaneous temperatures produced every hour by the HARMONIE-AROME model were compared with the observed temperatures of 74 sites. Comparison was performed with all HARMONIE-AROME based temperatures and observed temperatures whose locations matched spatially in a way that the observation site was located inside the area of modelled temperature grid cell. HARMONIE-AROME produces 2 m temperature for the whole grid cell. In addition, it produces 2 m temperature for the town and nature parts of the grid cell. We focus on the average temperature of the whole grid cell, as it is commonly the most used output of the model. Town and nature temperatures are used as examples in some comparisons, and when they are referred, it is specifically mentioned in the text.

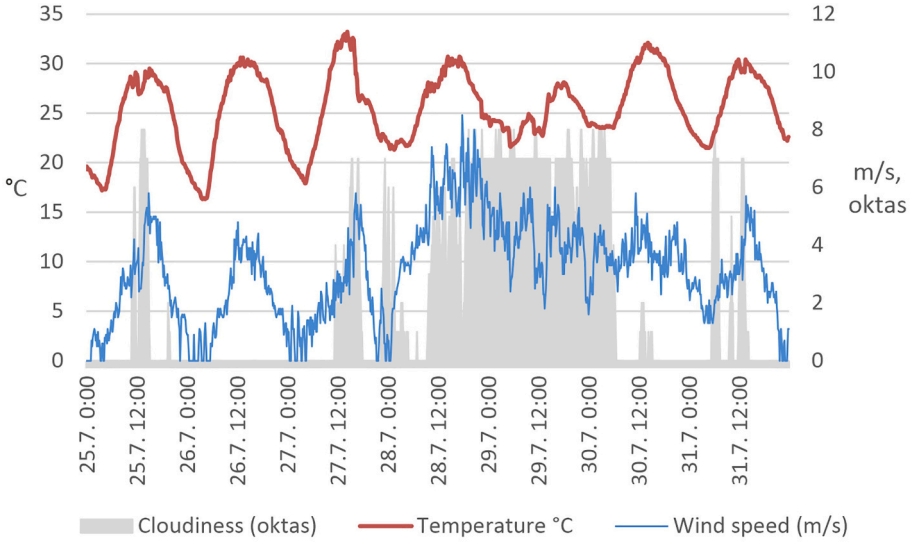

Fig. 4. Cloudiness, temperature and wind speed in Turku Artukainen weather station during the study period 25.-31.7.2018.

2.8. Evolution of weather during the study period

During the first part of the period 25.-31.7.2018, the weather in southwestern Finland was influenced by a high pressure ridge extending over the country from the east. Except for a brief spell of unsettled weather on the 29th and 30th of July, skies were mostly clear in the area and the temperature followed a well-defined daily course, with maximum temperatures close to 30 °C, and minimum temperatures between around 20 °C (Fig. 4). The average temperature in Turku Artukainen weather station, located ca. 5 km to the west of the city centre, during the period was 25.4 °C. Owing to the irregular cloud cover and wind on the 29th and 30th, the even daily march of the temperature was replaced by more irregular variation of a lesser amplitude, to be restored again on the 31th.

3. Results

3.1. Comparison of ECOCLIMAP-SG and CLC classifications

Of the tested 21 ECO-SG cover types that are present in the study area, correlation of the PGD cover types with the corresponding CORINE class(es) was statistically significant ($p \leq 0.01$) in case of 16 cover types (Table 1). Of the 16 statistically significant correlations, 15 were positive indicating a good spatial match between the ECO-SG and CORINE classifications. The correlation was strongest for the classes representing natural unbuilt land cover types, such as seas and oceans ($r = 0.971$), fields of winter C3 crops ($r = 0.880$) and forests of boreal needleleaf evergreen trees ($r = 0.841$). Of the ECO-SG cover types representing built areas, correlation was strongest for sparsely built areas ($r = 0.726$), large low-rise building areas ($r = 0.594$) and heavy industry areas ($r = 0.479$).

3.2. Spatial and land cover specific distribution of modelled temperatures

Regarding land areas, in nature-town dimension, the impact of the city was manifested in higher modelled average, daily minimum and daily maximum temperatures of areas determined as town compared to the areas defined as nature (Fig. 5). Of the urban land covers, average and daily minimum temperatures were highest in areas presented by LCZ10 (heavy industry), whereas daily maximum temperatures were highest in LCZ8 (large low-rise) areas. Of the water bodies, sea areas are characterised by small diurnal temperature range compared to other water areas and land areas. The most noteworthy feature is clearly lower daily maximum temperature compared to other water areas and land areas.

Concerning the spatial temperature differences of the study area as a whole, the UHIs of the Turku and Salo city centres are well detected. Salo is located approximately 50 km to the east of Turku. Local heat islands exist also eg. in the Turku dockyard area approximately 7 km to the west of the Turku city centre and in the areas to the north of the Turku city centre. In the sea areas, temperature gets slightly cooler towards the outer archipelago (Fig. 6).

Table 1
Pearson's correlation coefficients between the ECOCLIMAP-SG cover types and corresponding CORINE class(es). Coefficients are calculated between the areal proportions of ECO-SG cover types in the PGD and the corresponding CORINE class inside the 750 m × 750 m grid cells. CORINE class codes represent raster values of level 4 classification in a 20 m × 20 m dataset.

ECOCLIMAP-SG cover type in the PGD	Corresponding CORINE class(es)	Pearson's r
1 (sea and oceans)	49	0.971**
2 (lakes)	48	0.797**
4 (bare land)	8, 9, 38, 44	0.085**
5 (bare rock)	39	−0.002
8 (temperate broadleaf deciduous)	23, 24	0.228**
12 (boreal needleleaf evergreen)	25, 26, 27	0.841**
13 (temperate needleleaf evergreen)	25, 26, 27	−0.052**
15 (shrubs)	18, 22	0.007
17 (temperate grassland)	15	−0.002
19 (winter C3 crops)	17, 19, 20	0.880**
20 (summer C3 crops)	17, 19, 20	0.425**
21 (C4 crops)	17, 19, 20	0.003
23 (flooded grassland)	41, 42, 43, 45, 46	0.523**
24 (LCZ1: compact high-rise)	41, 42, 43, 45, 46	0.278**
25 (LCZ2: compact midrise)	1, 3, 5	0.265**
26 (LCZ3: compact low-rise)	1, 3, 5	0.137**
28 (LCZ5: open midrise)	1	−0.001
29 (LCZ6: open low-rise)	2	0.102**
31 (LCZ8: large low-rise)	4, 6	0.594**
32 (LCZ9: sparsely built)	2, 13	0.726**
33 (LCZ10: heavy industry)	4, 6	0.479**

** = correlation is statistically significant ($p \leq 0.01$).

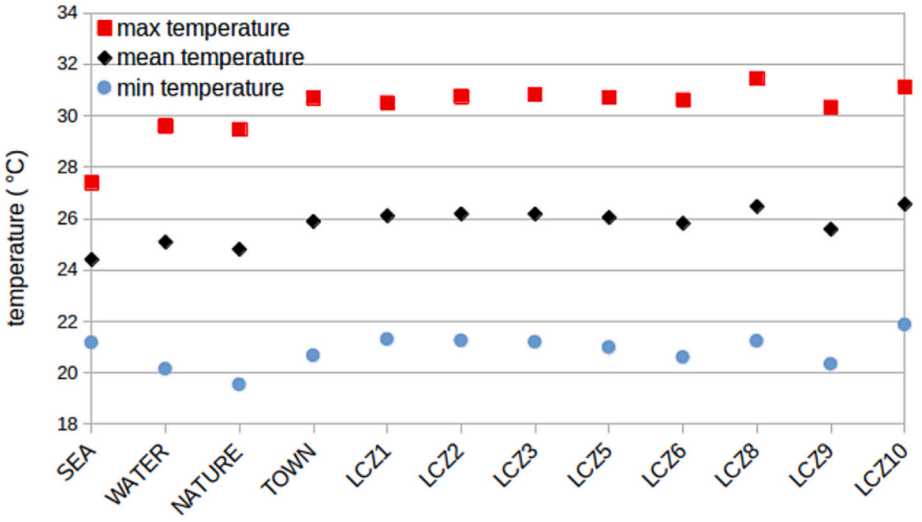

Fig. 5. The weighted average daily maximum, daily mean, and daily minimum modelled temperatures for each tile type and for urban cover types of ECOCLIMAP-SG in the study area. The weighted average temperatures are calculated from daily temperatures of the one week period 25.-31.7.2018 using the PGD grid cell tile/cover percentages as weights.

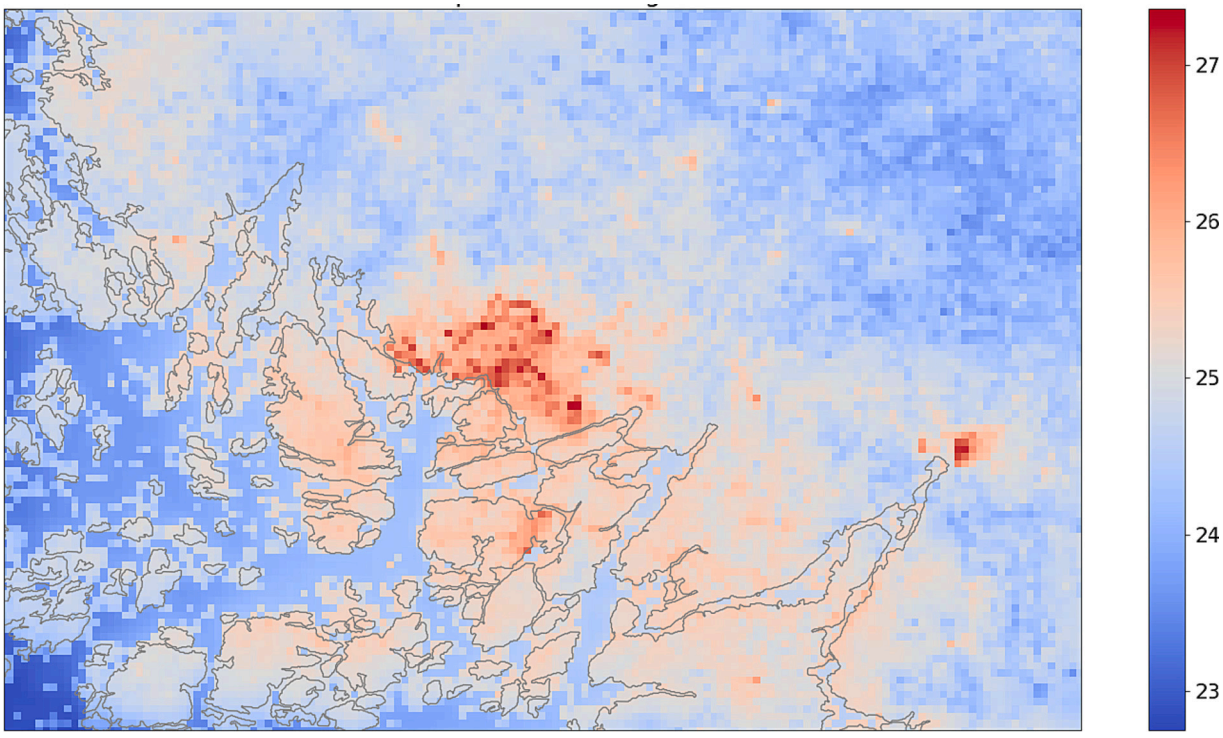

Fig. 6. The 750 m × 750 m resolution average temperature (°C) in the Turku area during the 25.-31.7.2018 heatwave as modelled by the HARMONIE-AROME model.

3.3. Difference between the modelled and observed temperatures

On the majority of the TURCLIM observation sites (68 sites out of 74) temperatures modelled by HARMONIE-AROME were on average warmer than the observed temperatures. On 6 sites, modelled temperatures were colder than observed (Fig. 7). Largest difference between the modelled and observed temperature occurred at the observation site Mylly, in which the observed temperatures were on average 2.12 °C colder than the modelled temperatures (site 50, Fig. 2 and Appendix B; see also Fig. 8). Of the sites in which the observed temperatures were warmer than modelled, the largest difference was on average 0.44 °C, observed in Kuuva, in the southernmost parts of the Ruissalo Island (site 66, Fig. 2 and Appendix B; see also Fig. 10).

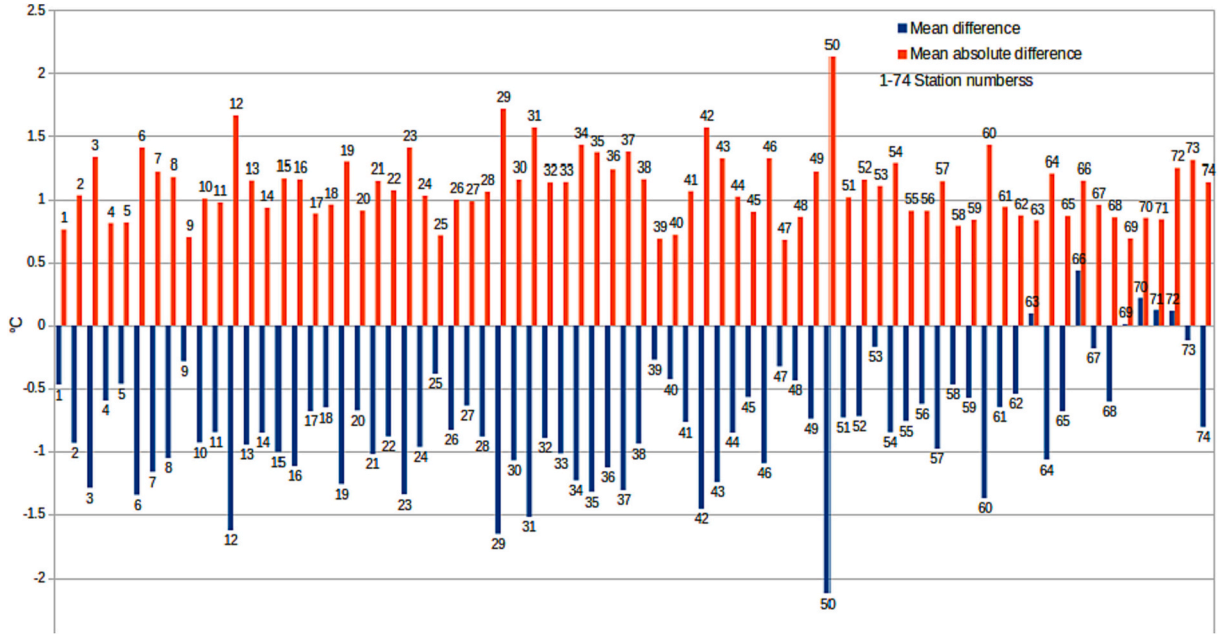

Fig. 7. Mean difference (blue) and mean absolute difference (orange) between mean observed temperature at TURCLIM stations and mean simulated temperature at the corresponding grid cell during the period 25.-31.7.2018. In the mean differences of the figure, modelled temperature is subtracted from the observed one. TURCLIM stations are in the order based on the distance from the city center (Number 1 is Kauppatori logger). All corresponding station logger numbers and respective logger names can be found in Appendix B, and logger locations in Fig. 2. (For interpretation of the references to colour in this figure legend, the reader is referred to the web version of this article.)

3.4. Spatial pattern of differences between modelled and observed temperatures

The sites with the largest difference between the modelled and observed temperatures are located in the suburban areas outside the grid plan area of the city centre. The sites are not concentrated in any specific area, and the differences between the modelled and observed temperatures can mostly be explained by microclimatic variability in the surroundings of the observation sites. The observation site with the largest difference, Mylly (Site 50, Fig. 2 and Appendix B; see also Fig. 8), is located in a grassy patch in the middle of large commercial buildings and asphalted areas, and consequently, do represent the microclimatic conditions of its immediate neighbourhood only, but not the densely built-up areas in the vicinity. In the PGD, the grid cell at the Mylly observation site is for its entire area covered by Local Climate Zone 8 characterised by large low-rise buildings and paved surfaces (see Stewart and Oke, 2012). Consequently, relatively high modelled temperatures in that specific grid cell can at least partly be explained by the fact that the model does not have information on the small grassy patch around the observation site, and thus models the temperature for built-up area, and not for grassy unbuilt area, in which the observation site is actually located. The site with second largest differences, 1.66 °C, Valkiasvuori, is located in the least built-up areas of the grid cell it represents (Site 29, Fig. 2 and Appendix B; see also Fig. 9). The buildings in the grid cell are mostly detached houses, and in the PGD the whole cell is classified as sparsely built. The Valkiasvuori observation site is located in a grassy area in the yard of a detached house. From southern and southwestern sides the site is bordered by a forested hill, resulting in less favourable radiative conditions and increased proneness to cold air drainage. These local characteristics could explain the large difference between the modelled and observed temperatures on that site. This is supported by the fact that in both cases (Mylly and Valkiasvuori) the modelled temperature for the nature part of the grid cell is on average closer to the observed temperature than the modelled temperature of the whole grid cell.

Of the observation sites in which the measured temperatures were higher than the modelled temperatures, the difference was largest in Kuuva (Site 66, Fig. 2 and Appendix B; see also Fig. 10). The site is located in the peninsula at the southest parts of the Ruissalo Island approximately 10 km to the SW of the Turku city centre. The south-facing slope in site surroundings consists of forested rocky ground. Distance to the coastline is approximately 20 m. Due to the topography, the observation site surroundings get rather a lot of solar radiation during the daytime, and part of it is stored into the rocky ground to be released in the evening and night. These environmental conditions probably result in the observation site surroundings to be the warmest area of the grid cell, that otherwise is mostly covered by the sea. In the PGD, the whole grid cell is classified as 'seas and oceans', and consequently, the HARMONIE-AROME's modelled temperature for Kuuva represents practically air temperature over the sea.

On average the best match between the modelled and observed temperatures (difference 0.009 °C) occurred in suburban site Jäkärlä (Site 69, Fig. 2 and Appendix B; see also Fig. 11). The respective grid cell area is rather homogenous, covered by detached houses and low blocks of flats, and interleaving vegetated areas. In the PGD, 93.3% of the grid cell area is classified as sparsely built, whereas 6.7% represents winter C3 crops. The observation site is located at the edge of the small asphalted parking site, surrounded by

Fig. 8. Mylly observation site and HARMONIE-AROME experiment grid. Background image: Orthophoto, 2020, National Land Survey of Finland.

grassy ground and sporadic trees. Distance to the nearest building is approximately 20 m. In general, the observation site represents well the land cover of the grid cell as a whole.

An example of a good match of the modelled and observed temperatures is also a Hiiriluoto, mäki observation site in the Ruissalo island (Site 53, Fig. 2 and Appendix B; see also Fig. 12), in which the modelled temperature was on average 0.17 °C warmer than the observed temperature. Similarly to the previous example, Jäkärlä, the land cover inside the PGD grid cell is rather homogenous, consisting of needleleaf or broadleaf forest (50%) and winter C3 crops (50%). Even if rather homogenous in land use, the grid cell area is of its northernmost part topographically relatively variable, and consequently, also a good example of inner grid cell differences in observed temperatures; during the 1-week long study period, the Hiiriluoto, mäki observation site is on average 0.56 °C warmer that the Hiiriluoto, manner observation site (Site 52, Fig. 2 and Appendix B; see also Fig. 12) about 210 m to the southeast of it. In daily minimum temperature the respective difference was 0.45 °C, and in daily maximum temperature 0.97 °C. Hiiriluoto, mäki site is located on the top of a hill on approximately 20 m higher position than the Hiiriluoto, manner site, which may explain the observed differences. Probably also a bedrock outcrop and related sparser forest immediately to the north of Hiiriluoto, mäki site causes more favourable radiative conditions compared to the surroundings of Hiiriluoto, manner site.

When assessing the differences between whole grid cell, nature and town temperatures of the selected observation sites presented

Fig. 9. Valkiasvuori observation site and HARMONIE-AROME experiment grid. Background image: Orthophoto, 2020, National Land Survey of Finland.

in Fig. 13, in majority of sites the whole grid cell temperature, and consequently also the difference from observed temperature, settles logically between the nature and town temperature. In site Mylly, noteworthy is the small difference between the town temperature and temperature of the whole grid cell, which for its part supports our assumption that the large difference between the modelled and observed temperature at that site is partly explained by the fact that the modelled temperature is practically the modelled temperature for the urban areas of the grid cell, and not that of the nature part of the grid cell, in which the observation site is located.

3.5. Diurnal pattern of differences between modelled and observed temperatures

As stated earlier, the modelled temperatures are on average warmer than the observed ones. Diurnally, the differences are generally

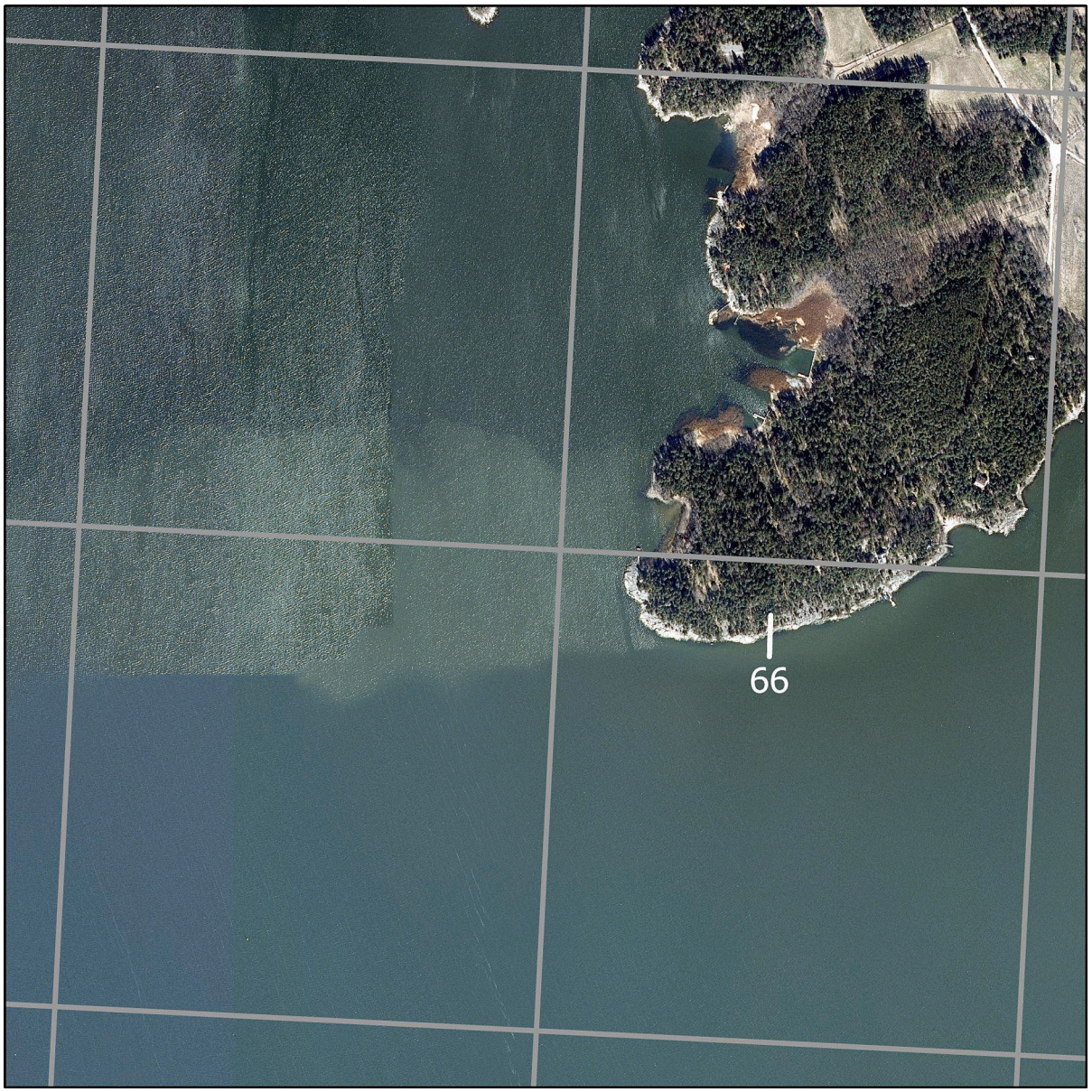

Fig. 10. Kuuva observation site and HARMONIE-AROME experiment grid. Background image: Orthophoto, 2020, National Land Survey of Finland.

largest at the times of daily minimum temperatures that in summer often occur early in the morning slightly after sunrise at around 4–5 am local solar time (UTC +2) (Fig. 14). In the daytime, the respective differences are smaller, but also then the modelled temperatures are principally warmer than the observed temperatures. Regarding the momentary spatial temperature range, in daytime the range is larger in modelled temperatures, whereas around the time of daily minimum temperatures, the range is larger in observed temperatures.

The diurnal profile of the difference between the modelled and observed temperatures of the site Mylly (site 50, Fig. 2 and Appendix B) in which the difference is on average largest, follows the same pattern than the respective difference of the observation sites in general, i.e. the modelled temperatures are higher than the observed, and the difference is largest for daily minimum temperatures (Fig. 15). This is, however, the case only in the beginning of the one-week period, whereas in the end of the period, modelled temperatures are also higher than the observed, but the difference is largest for daily maximum temperatures. A similar kind of change, although not as clear, is seen also more generally (see Fig. 14).

Fig. 11. Jäkärlä observation site and HARMONIE-AROME experiment grid. Background image: Orthophoto, 2020, National Land Survey of Finland.

A diurnal variation of differences between the modelled and observed temperatures in Jäkärlä (site 69, Fig. 2 and Appendix B), in which the difference is on average smallest, follows the pattern of the respective variation in general and that of the large differences' site Mylly, as far as daily minimum temperatures are considered, i.e. the modelled temperatures are higher than the observed temperatures (Fig. 16). The difference is, however, very small, and at one night of the one-week long study period, the modelled and observed temperatures are practically the same. Clearest difference to the general pattern and especially to the pattern of the site Mylly occurs in daily maximum temperatures, in which the observed temperatures are principally higher than the modelled temperatures, especially during the first days of the study period. To summarize, the good match between the modelled and observed temperatures in Jäkärlä is in a diurnal profile manifested as a generally small difference whose direction varies depending on the time of the day.

Fig. 12. Hiiriluoto, mäki (site 53) and Hiiriluoto, manner (site 52) observation sites and HARMONIE-AROME experiment grid. Background image: Orthophoto, 2020, National Land Survey of Finland.

4. Discussion

As a preliminary step of the study, representativeness of the ECOCLIMAP-SG based land cover dataset, the PGD, in the study area was estimated by means of CORINE Land Cover dataset. The highest positive correlation coefficients indicating good spatial match between the ECO-SG and CORINE classifications occurred with natural unbuilt land cover types, such as sea areas, fields and forests. For built-up areas, correlation was lower, but without one exception statistically significant and positive. The weaker correlation of built ECO-SG cover types with the corresponding CORINE classes, compared to the unbuilt areas, does seem to principally reflect the differences of the ECO-SG and CORINE classifications, and consequently, cannot be interpreted as a sign of mismatch between the ECO-SG cover types and the actual land cover in the built-up areas. For example, in the grid plan area of the Turku city centre, four ECO-SG

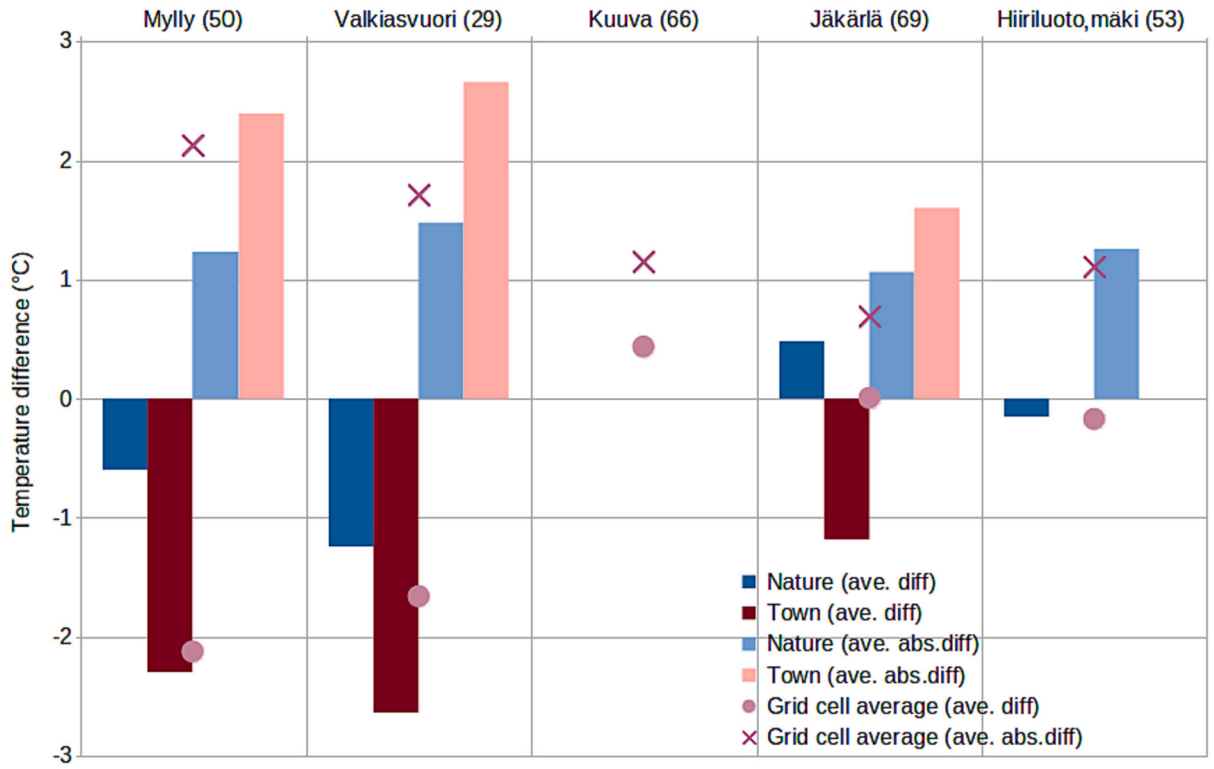

Fig. 13. Average differences (observed minus modelled) and average absolute differences between the town (TEB), nature (ISBA), and grid cell average temperatures of the HARMONIE-AROME simulation and observed temperatures of selected stations. Mylly site is located in an urban area, while Valkiasvuori and Jäkärlä represent semi-urban areas. Hiiriluoto, mäki represents rural environment, whereas Kuuva's grid cell is determined for its whole area as 'seas and oceans' cover type in the PGD. Consequently, it doesn't have either modelled nature or town temperature.

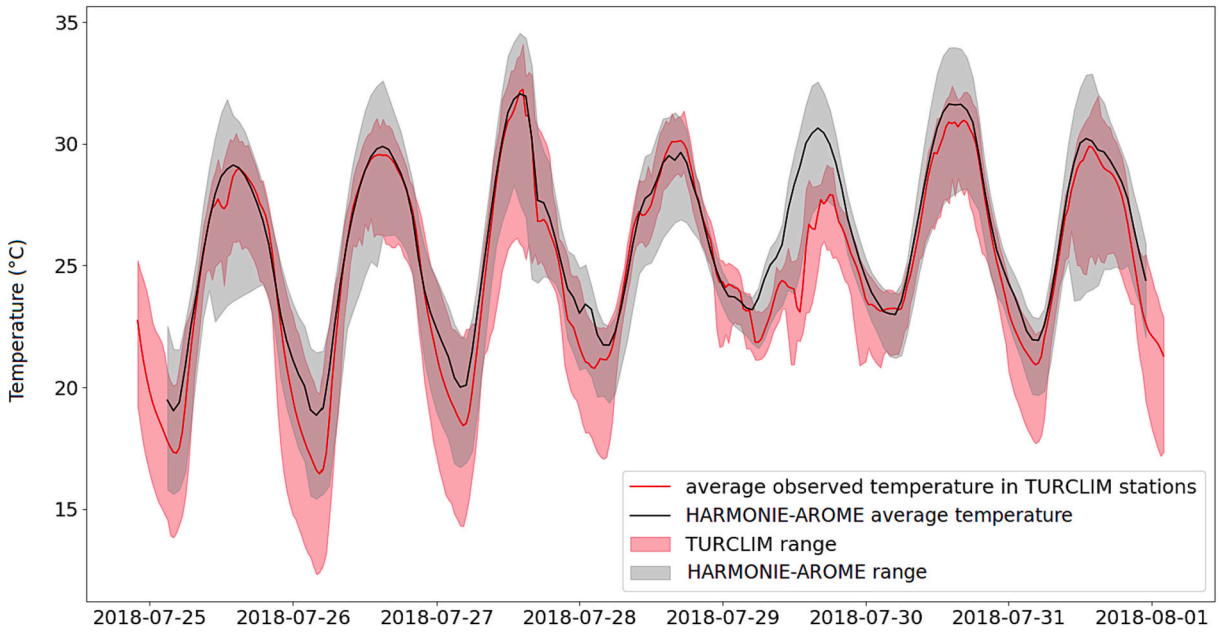

Fig. 14. Diurnal ranges of observed temperatures from TURCLIM stations and simulated HARMONIE-AROME temperatures of the corresponding grid cells.

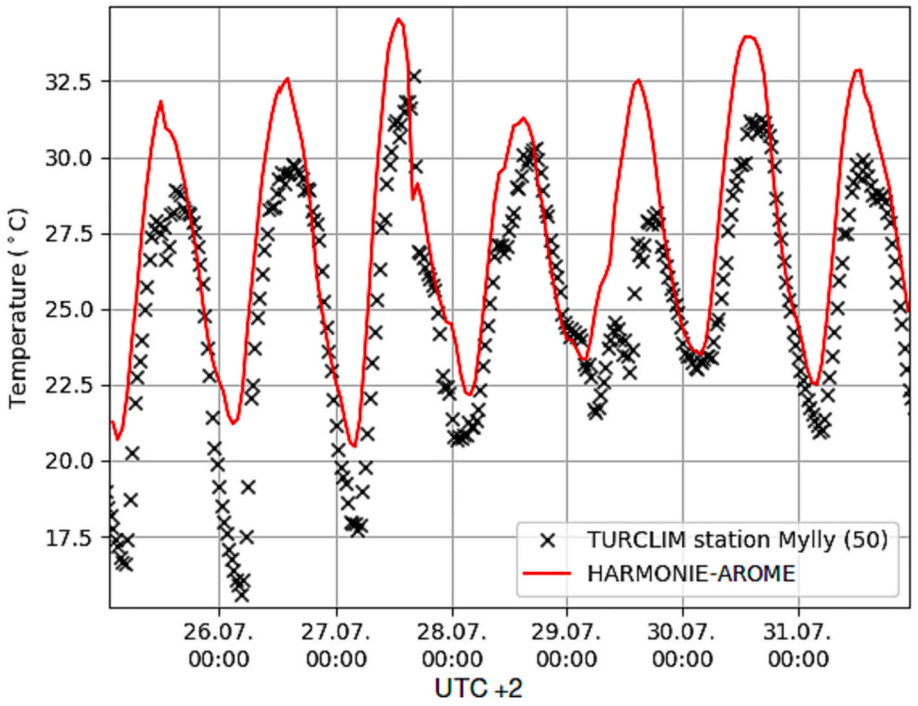

Fig. 15. Diurnal cycles of observed temperature at the Mylly station (the site with the largest differences between modelled and observed temperatures) and the HARMONIE-AROME temperature of the corresponding grid cell in 25.-31.7.2018.

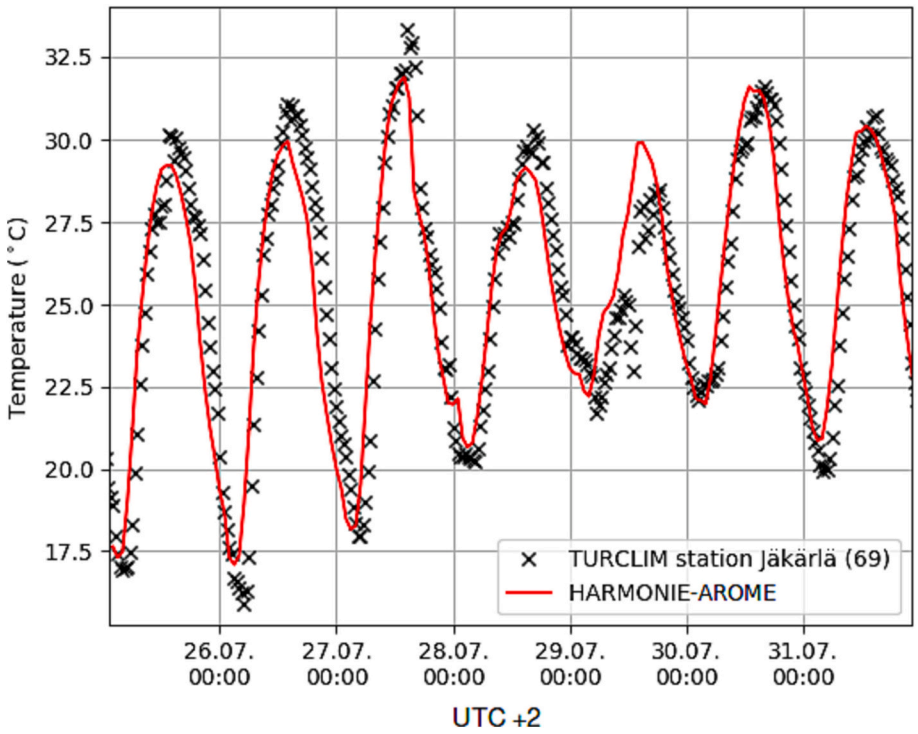

Fig. 16. Diurnal cycles of observed temperature at the Jäkärlä station (the site with the smallest differences between the modelled and observed temperatures) and the HARMONIE-AROME temperature of the corresponding grid cell.

cover types representing built-up areas are rather widely present, whereas in the case of CORINE classification, the respective areas are mostly covered by two CORINE classes only. Whereas built-up classes of CORINE rather clearly make a difference between the uses of the built areas (e.g. commercial units, road and rail networks and associated land, summer cottages), built-up cover types of ECO-SG do in more detail reflect the differences of building sizes and building density. As both building size and type (e.g. residential, commercial) affect the amount of anthropogenic heat release (Quah and Roth, 2012; Sailor et al., 2015), from that perspective neither the CORINE nor the ECO-SG classification can straightforwardly be considered more suitable for urban temperature modelling purposes. Considering the things beyond the classification typology, CORINE's benefit is its high spatial resolution (20 m).

Even if the relatively low correlations of single ECO-SG's built-up cover types can mostly be explained by the differences between the ECO-SG and CORINE classifications, from local climate point of view, the HARMONIE-AROME experiment's physiographic dataset has some weaknesses related to the resolution and some land cover types. The PGD includes information on areal proportions of each land cover class inside each 750 m $\times$ 750 m grid cell, but it lacks information on where inside the grid cell the specific land use types are located. In addition, for each cell, there's a minimum threshold proportion that has to be covered by a single land cover type in order to be shown in the data. The 300 m resolution source data that form a basis of 750 m resolution dataset, only include information on the most dominant land cover type (CNRM, 2018) and consequently, the land cover types that cover only small areas, are not visible in the 750 m resolution dataset. Regarding the weaknesses related to certain land cover types, in the Turku area, on a sample basis, in the areas in which the large asphalted roads cross the uninhabited field and forest areas, the 750 m PGD grid cells often do not include any proportions of built land cover classes that would reflect the local heating impact of dark asphalt roads and the traffic on them. This may be either due to the relatively low proportion of the road area inside a grid cell, or due to the ECO-SG classification that does not have an appropriate class for the asphalted roads that cross the uninhabited regions.

On average, the HARMONIE-AROME temperatures were higher than the observed temperatures. The differences, however, were site-dependent, and both over- and underestimation of temperatures existed. Similar general warm bias with site-specific exceptions of cold bias has been observed also by Amorim et al. (2020) when modelling the Stockholm's air temperatures with HARMONIE-AROME model. Site-dependent dichotomy was observed also by Quitián-Hernández et al. (2021), who compared the HARMONIE-AROME 2 m temperatures with the observed temperatures of six sites in Canary Islands, Madeira and Azores during the subtropical cyclone in October 2014. In their study, however, opposite to the experiences in Turku and Stockholm, in the majority of sites, cold bias occurred.

In the study of Amorim et al. (2020), the differences between the observed temperatures and HARMONIE-AROME based temperatures were larger in rural than in urban areas. In our study, the largest or smallest differences were not spatially concentrated in certain areas, but were mostly related to the internal heterogeneity/homogeneity of the grid cell at the locations of the observation sites, and to the fact that how well did the immediate surroundings of the observation site represented the land use and topography of the grid cell as a whole. It is not surprising that the largest differences between the TURCLIM observations and model simulations are found in areas where the TURCLIM logger is located in a small vegetated area surrounded by dense urban area. In the case of the Mylly logger (site 50, Fig. 2 and Appendix B; see also Fig. 8), the vegetated area is too small to be accounted for in the PGD, but it dominates the micro climate at the logger site. When taking into account the urban heat island effect and the fact that many numerical weather prediction models tend to overestimate night time temperatures, the large differences are almost guaranteed (Iriza et al., 2016). In sites like Jäkärlä (site 69, Fig. 2 and Appendix B; see also Fig. 11), on the contrary, where the logger is inside a homogeneous grid cell in terms of actual land use and ECO-SG covers, the difference between simulated and observed temperature is rather small.

The fact that in the Mylly observation site the modelled-observed differences in daily minimum temperatures were largest in the beginning of the study period when the wind speed was as it weakest or even zero enabling sharp spatial temperature differences, supports the assumption that the grid cell heterogeneity and, consequently, limited spatial representativeness of the observation site explain the poor match between the modelled and observed night-time temperature. Stable atmospheric stratification and related calm or weak wind conditions that often occur at nights, have been challenging for the HARMONIE-AROME model and numerical weather prediction models in general, and hence, the larger difference between the modelled and observed temperatures in the beginning of the study period could be explained partly also by this case-sensitivity of the model performance (Sandu et al., 2013; Kalverla et al., 2019; Sekula et al., 2019).

In an ideal case, the actual measured temperature should be between simulated nature and town temperatures, as urban areas have a warming effect. This is not always the case and in some cases the nature temperature is on average higher than observed temperature (for example sites Mylly (50) and Valkiasvuori (29) in Fig. 13).This can also be explained by the too warm town temperatures. The separate tiles (nature, town, water bodies) are treated independently, but they do interact indirectly, via the atmosphere. In this range, nearby buildings have a significant warming effect, and this may be seen also in the nature temperature on the surface. When nature temperature is on average colder than the observation, the overall difference seems to be relatively small. Jäkärlä is a good example of this, as seen in Fig. 13.

Regarding the diurnal pattern of differences in modelled and observed temperatures, the differences were generally larger at night than during the daytime. The modelled daily minimum temperatures were systematically higher than the observed ones, whereas in daily maximum temperatures the difference between the modelled and observed temperatures was small. According to our modelled and observed data (not shown here), the night-time positive bias in temperature was often accompanied with negative bias in relative humidity, as expected. Similar kind of pattern for numerical weather prediction model to overestimate the nocturnal temperatures has been observed also in topographically varying areas by Sekula et al. (2019). Regarding urban areas, analogous results were observed by the predictions of dynamical urban climate model MUKLIMO_3 by Hollósi et al. (2021). At the same study, however, the numerical weather predicting model ALARO that was coupled with the MUKLIMO_3 model, behaved differently, as the modelled and observed temperatures deviated mostly during daytime.

Based on our experiences on the HARMONIE-AROME model performance in the topographically alternating coastal city, one target

for development is spatial resolution; 750 m is too coarse for detecting sharp spatial temperature differences that are typical for highly varying areas during weak wind conditions and/or stable atmospheric stratification. The higher computational demand, however, limits the possibilities to use smaller grid cell size. Regardless of the resolution, appropriate definition and quantification of land surface characteristics and topography are essential for model performance. Consequently, we recommend evaluating these factors and their roles in model performance case-specifically for model development purposes. Already earlier recognised challenges in model performance during weak wind and stable atmospheric conditions were present also in this study calling for its part better modelling of the stable boundary layer.

5. Conclusions

Based on this study, we conclude that:

1) ECOCLIMAP Second Generation land cover classification does in general reflect well the land cover in the study area, in the 750 m resolution of the PGD. The spatial correspondence with CORINE land cover is best in natural uninhabited land cover types, but also good in built environments. The weaker correspondence in built areas is mostly due to the differences between the classification principals, not due to the impresentability of the ECO-SG classification. Regarding specific land cover types, asphalted roads in uninhabited field and forest areas were poorly represented in the PGD.
2) During the one-week long summer period, the temperatures modelled by HARMONIE-AROME model were on average 0.8 °C warmer than the observed temperatures in the areas of the respective grid cells. Highest site-specific difference to the same direction was 2.12 °C, and to the opposite direction 0.44 °C.
3) Largest differences between the modelled and observed temperatures are not concentrated in any specific area, but common to them is that they occurred at the sites in which the grid cell areas are inhomogeneous in land use and topography, and the observation site surrounding does poorly represent the land cover and/or topographic conditions of the grid cell area as a whole. Logically, the best match between the modelled and observed temperatures occurred at the sites in which the observation site surrounding represents well the land cover and topographic conditions of the respective grid cell area.
4) Diurnally, differences between the modelled and observed temperatures were largest for the daily minimum temperatures, whereas for the daily maximum temperatures the match between the modelled and observed temperatures was principally good. In daily minimum temperatures, the dominant feature was that the modelled temperatures were higher than the observed temperatures.

CrediT authorship contribution statement

Juuso Suomi: Conceptualization; Data curation; Formal analysis; Funding acquisition; Investigation; Methodology; Validation; Visualization; Writing - original draft; Writing - review & editing.

Olli Saranko: Conceptualization; Formal analysis; Investigation; Resources; Software; Validation; Visualization; Writing - original draft; Writing - review & editing.

Antti-Ilari Partanen: Conceptualization, Writing - review & editing, Supervision, Project administration, Funding acquisition.

Carl Fortelius: Conceptualization; Writing - review & editing.

Carlos Gonzales-Inca: Conceptualization; Methodology; Writing - original draft; Writing - review & editing.

Jukka Käyhkö: Conceptualization; Methodology; Writing - Review & Editing; Supervision; Project administration; Funding acquisition.

Declaration of competing interest

The authors declare that they have no competing financial interests or personal relationships that could have influenced the work reported in this paper.

Data availability

The data will be made available on request as widely as possible

Acknowledgements

We thank the Geography Section of the University of Turku and Urban Environment Division of the City of Turku for financial support in maintaining the TURCLIM weather observation network. We thank the Finnish Meteorological Institute for open access weather data. The HARMONIE-AROME model integrations were carried out using the computing resources of the ECMWF. Financial support for all authors for this research was granted by the Research Council of Finland (the consortium acronym HERCULES, decision numbers 329235 and 329241).

Appendix A. Information on CORINE Land Cover classification

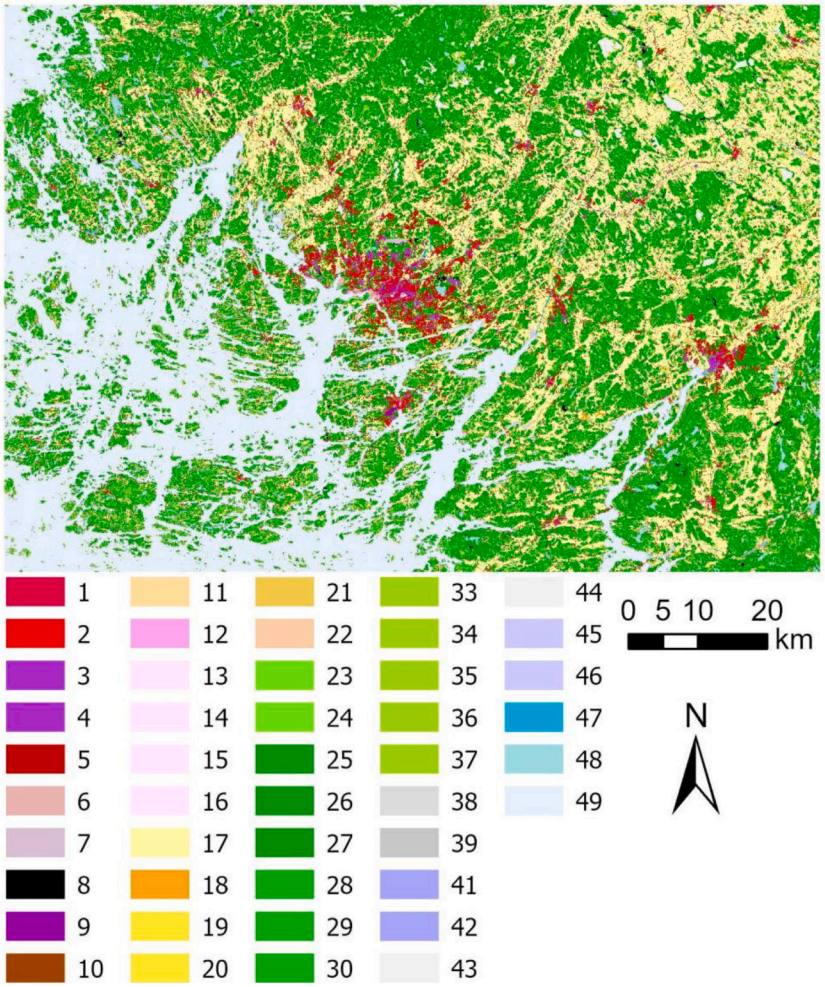

Fig. A.1. Corine Land Cover (CLC) 2018 map of the study area. The map represents the most detailed level 4 classification. For information on the class codes and respective class descriptions, see Table A.1.

Table A.1
Corine Land Cover (CLC) 2018 level 4 class codes and respective class descriptions. For information on spatial coverage of the classes in the study area, see Fig. A.1.

Class code	Class description
1	Continuous urban fabric
2	Discontinuous urban fabric
3	Commercial units
4	Industrial units
5	Road and rail networks and associated land
6	Port areas
7	Airports
8	Mineral extraction sites
9	Open cast mines
10	Dump sites
11	Construction sites
12	Green urban areas
13	Summer cottages
14	Sport and leisure areas
15	Golf courses
16	Racecourses
17	Non-irrigated arable land
18	Fruit trees and berry plantations
19	Pastures
20	Natural pastures

(*continued on next page*)

Table A.1 (*continued*)

Class code	Class description
21	Arable land outside farming subsidies
22	Agro-forestry areas
23	Broad-leaved forest on mineral soil
24	Broad-leaved forest on peatland
25	Coniferous forest on mineral soil
26	Coniferous forest on peatland
27	Coniferous forest on rocky soil
28	Mixed forest on mineral soil
29	Mixed forest on peatland
30	Mixed forest on rocky soil
31	Natural grassland
32	Moors and heathland
33	Transitional woodland/shrub, cc <10%
34	Transitional woodland/shrub, cc 10–30%, on mineral soil
35	Transitional woodland/shrub, cc 10–30%, on peatland
36	Transitional woodland/shrub, cc 10–30%, on rocky soil
37	Transitional woodland/shrub under power lines
38	Beaches, dunes, and sand plains
39	Bare rock
40	Sparsely vegetated areas
41	Inland marshes, terrestrial
42	Inland marshes, aquatic
43	Peatbogs
44	Peat production sites
45	Salt marshes, terrestrial
46	Salt marshes, aquatic
47	Water courses
48	Water bodies
49	Sea and ocean

Appendix B. Information on the temperature observation sites

Table B.1
Characteristics of the TURCLIM observation sites. For information on the observation site locations, see Fig. 2. Observation site numbers in the table correspond with the numbers in the respective figure.

Site name	Site number	Distance (km) from the city centre	Elevation (m above sea) level)	Most common land cover type inside 100 m buffer**
Kauppatori*	**1**	**0.0**	**7.7**	**Commercial units**
Puolalanmäki	**2**	**0.3**	**28.9**	**Commercial units**
Puutori	**3**	**0.3**	**18.1**	**Commercial units**
Betel	**4**	**0.3**	**16.9**	**Commercial units**
Virastotalo	**5**	**0.8**	**7.2**	**Commercial units**
Piispankatu	**6**	**0.9**	**9.7**	**Discontinuous urban fabric**
Rautatieasema	**7**	**0.9**	**9.7**	**Road and rail networks and associated land**
Yliopistonmäki	**8**	**1.0**	**35.6**	**Commercial units**
Kerttuli	**9**	**1.0**	**23.0**	**Continuous urban fabric**
Mikaelinkirkko	**10**	**1.0**	**9.8**	**Commercial units**
Urheilupuisto	**11**	**1.1**	**23.3**	**Sport and leisure areas**
Kähäri	**12**	**1.2**	**20.9**	**Discontinuous urban fabric**
Saarnitie	**13**	**1.3**	**16.8**	**Discontinuous urban fabric**
Sirkkala	**14**	**1.3**	**23.1**	**Commercial units**
Martti	**15**	**1.4**	**2.5**	**Continuous urban fabric**
Rieskalähde	**16**	**1.6**	**31.4**	**Discontinuous urban fabric**
Kupittaa	**17**	**1.6**	**17.3**	**Sport and leisure areas**
Alfa	**18**	**1.7**	**21.0**	**Commercial units**
Kakola	**19**	**1.9**	**18.0**	**Commercial units**
Ylioppilaskylä	**20**	**2.1**	**15.2**	**Discontinuous urban fabric**
Uudenmaantie	**21**	**2.2**	**24.2**	**Discontinuous urban fabric**
Nummi	**22**	**2.6**	**29.9**	**Discontinuous urban fabric**
Halinen	**23**	**2.6**	**7.5**	**Commercial units, water courses**
Luolavuori	**24**	**2.7**	**43.5**	**Coniferous forest on mineral soil**
Linna	**25**	**2.8**	**2.3**	**Port areas**
Suikkila	**26**	**2.8**	**22.2**	**Commercial units**
Heikkilän kasarmi	**27**	**2.9**	**4.1**	**Transitional woodland/shrub, cc 10–30%, on mineral soil**

(*continued on next page*)

Table B.1 (*continued*)

Site name	Site number	Distance (km) from the city centre	Elevation (m above sea level)	Most common land cover type inside 100 m buffer**
Ispoinen	28	3.0	16.5	Discontinuous urban fabric
Valkiasvuori	29	3.0	29.7	Discontinuous urban fabric
Vapaavarasto	30	3.2	2.5	Port areas
Impivaara	31	3.2	31.1	Transitional woodland/shrub, cc 10–30%, on mineral soil
Liponkuja	32	3.4	22.7	Discontinuous urban fabric
Hautausmaa	33	3.5	24.9	Commercial units
Pääskyvuori, laakso	34	3.5	15.2	Transitional woodland/shrub, cc 10–30%, on mineral soil
Kristillinen	35	3.6	21.6	Discontinuous urban fabric
Metsäkylä	36	3.6	22.5	Mixed forest on mineral soil
Marjaniemi	37	3.9	17.0	Commercial units
Ryhmäpuutarha	38	3.9	13.8	Transitional woodland/shrub, cc 10–30%, on mineral soil
Pääskyvuori	39	3.9	47.7	Discontinuous urban fabric
Runosmäki	40	4.1	37.6	Commercial units
Kurala	41	4.2	13.5	Non-irrigated arable land
Huhkola	42	4.4	18.8	Non-irrigated arable land
Vahdontie	43	4.5	40.1	Road and rail networks and associated land
Messukeskus	44	4.6	6.0	Commercial units
Katariina	45	4.8	6.5	Non-irrigated arable land
Hirvensalo	46	5.1	0.8	Non-irrigated arable land
Varissuo	47	5.1	46.2	Continuous urban fabric
Ruissalo	48	5.2	1.0	Arable land outside farming subsidies
Kasvitieteellinen	49	5.5	4.6	Green urban areas
Mylly	50	5.5	20.8	Road and rail networks and associated land
Perno	51	6.0	10.1	Commercial units
Hiiriluoto, manner	52	6.2	17.3	Mixed forest on mineral soil
Hiiriluoto, mäki	53	6.2	36.3	Coniferous forest on mineral soil
Hiiriluoto, ranta	54	6.2	0.5	Salt marshes, terrestrial
Rauhanniemi	55	6.4	39.7	Discontinuous urban fabric
Raisio	56	6.8	14.5	Continuous urban fabric
Pansio	57	7.2	3.5	Coniferous forest on mineral soil
Vanhalinna	58	7.4	22.2	Non-irrigated arable land
Metsämäki	59	7.4	21.3	Non-irrigated arable land
Kaarina	60	8.3	17.3	Commercial units
Satava	61	8.4	1.2	Sport and leisure areas, Mixed forest on mineral soil
Camping	62	9.8	1.4	Sport and leisure areas
Ylijoki	63	9.8	33.8	Non-irrigated arable land
Niuskala	64	9.8	32.4	Coniferous forest on mineral soil
Kakskerta	65	9.9	16.3	Golf courses
Kuuva	66	9.9	4.8	Coniferous forest on mineral soil
Kolkka	67	10.0	0.5	Salt marshes, aquatic
Tuorla	68	10.4	14.1	Non-irrigated arable land
Jäkärlä	69	11.0	56.6	Continuous urban fabric
Lieto	70	13.9	30.8	Non-irrigated arable land
Sikilä	71	18.1	43.3	Arable land outside farming subsidies
Kuusinen	72	30.2	1.5	Sea and ocean
Karinainen	73	37.4	67.7	Non-irrigated arable land
Kirjainen	74	40.9	8.8	Coniferous forest on mineral soil

* **Observation site Kauppatori (site number 1) at the north-western side of the marketplace is considered a city centre.**

** **Land cover type represents the Corine Land Cover 2018 dataset's level 4 class that covers the largest area inside a 100 m radius buffer around the observation site.**

References

ACCORD, 2022. A consortium for COnvention-scale modelling Research and Development. http://www.umr-cnrm.fr/accord (accessed 9 December 2021).

Alalammi, P., 1987. Atlas of Finland: 131, Climate. National board of survey, Geographical society of Finland.

Amorim, J.H., Segersson, D., Körnich, H., Asker, C., Olsson, E., Gidhagen, L., 2020. High resolution simulation of Stockholm's air temperature and its interactions with urban development. Urban Clim. 32, 100632 https://doi.org/10.1016/j.uclim.2020.100632.

Atkinson, B.W., 2003. Numerical modelling of urban Heat-Island intensity. Bound.-Layer Meteorol. 109, 285–310. https://doi.org/10.1023/A:1025820326672.

Aune-Lundberg, L., Strand, G.-H., 2021. The content and accuracy of the CORINE land cover dataset for Norway. Int. J. Appl. Earth Obs. Geoinf. 96, 102266 https://doi.org/10.1016/j.jag.2020.102266.

Bahi, H., Mastouri, H., Radoine, H., 2020. Review of methods for retrieving urban heat islands. Mater. Today: Proc. 27 (4), 3004–3009. https://doi.org/10.1016/j.matpr.2020.03.272.

Bengtsson, L., Andrae, U., Aspelien, T., Batrak, Y., Calvo, J., Rooy, W.C., Gleeson, E., Hansen-Sass, B., Homleid, M., Hortal, M., Ivarsson, K., Lenderink, G., Niemelä, S., Nielsen, K.P., Onvlee, J., Rontu, L., Samuelsson, P., Muñoz, D.S., Subias, Á., Tijm, S., Toll, V., Yang, X., Køltzow, M., 2017. The HARMONIE-AROME model configuration in the ALADIN-HIRLAM NWP system. Mon. Weather Rev. 145, 1919–1935. https://doi.org/10.1175/MWR-D-16-0417.1.

Bhargava, A., Lakmini, S., Bhargava, S., 2017. Urban Heat Island effect: It's relevance in urban planning. J. Biodivers. Endanger. Species 5, 187. https://doi.org/10.4172/2332-2543.1000187.

Burger, M., Gubler, M., Heinimann, A., Brönnimann, S., 2021. Modelling the spatial pattern of heatwaves in the city of Bern using a land use regression approach. Urban Clim. 38, 100885 https://doi.org/10.1016/j.uclim.2021.100885.

CNRM, 2018. Wiki – ECOCLIMAP-SG – CNRM Open Source Site. https://opensource.umr-cnrm.fr/projects/ecoclimap-sg/wiki (accessed 15 June 2021).

Copernicus, 2021. CORINE Land Cover. https://land.copernicus.eu/pan-european/corine-land-cover (accessed 14 September 2021).

de Bode, M., Hedde, T., Roubin, P., Durand, P., 2023. A method to improve land use representation for weather simulations based on high-resolution data sets—application to Corine land cover data in the WRF model. Earth Space Sci. 10 https://doi.org/10.1029/2021EA002123 e2021EA002123.

DuchÊne, F., Van Schaeybroeck, B., Caluwaerts, S., De Troch, R., Hamdi, R., Termonia, P., 2020. A statistical–dynamical methodology to downscale regional climate projections to urban scale. J. Appl. Meteorol. Climatol. 59 (6), 1109–1123. https://doi.org/10.1175/JAMC-D-19-0104.1.

Elliott, H., Eon, C., Breadsell, J.K., 2020. Improving City vitality through urban heat reduction with green infrastructure and design solutions: a systematic literature review. Buildings 10 (12), 219. https://doi.org/10.3390/buildings10120219.

Emery, J., Pohl, B., Crétat, J., Richard, Y., Pergaud, J., Rega, M., Zito, S., Dudek, J., Vairet, T., Joly, D., Thévenin, T., 2021. How local climate zones influence urban air temperature: measurements by bicycle in Dijon, France. Urban Clim. 40, 101017 https://doi.org/10.1016/j.uclim.2021.101017.

Fenner, D., Holtmann, A., Meier, F., Langer, I., Scherer, D., 2019. Contrasting changes of urban heat island intensity during hot weather episodes. Environ. Res. Lett. 14, 124013 https://doi.org/10.1088/1748-9326/ab506b.

GHSL, 2022. Global Human Settlement Layer. Open and free data and tools for assessing the human presence on the planet. https://ghsl.jrc.ec.europa.eu/. (Accessed 19 August 2021).

Hollósi, B., Žuvela-Aloise, M., Oswald, S., Kainz, A., Schöner, W., 2021. Applying urban climate model in prediction mode—evaluation of MUKLIMO_3 model performance for Austrian cities based on the summer period of 2019. Theor. Appl. Climatol. 144, 1181–1204. https://doi.org/10.1007/s00704-021-03580-6.

Imran, H.M., Shammas, M.I., Rahman, A., Jacobs, S.J., Ng, A.W.M., Muthukumaran, S., 2021. Causes, modeling and mitigation of urban Heat Island: a review. Earth Sci. 10 (6), 244–264. https://doi.org/10.11648/j.earth.20211006.11.

Iriza, A., Dumitrache, R.C., Lupascu, A., Stefan, S., 2016. Studies regarding the quality of numerical weather forecasts of the WRF model integrated at high-resolutions for the Romanian territory. Atmósfera 29 (1), 11–21. https://doi.org/10.20937/ATM.2016.29.01.02.

Jokinen, P., Pirinen, P., Kaukoranta, J.-P., Kangas, A., Alenius, P., Eriksson, P., Johansson, M., Wilkman, S., 2021. Tilastoja Suomen ilmastosta ja merestä 1991–2020 (climatological and oceanographic statistics of Finland 1991–2020). Raportteja 2021, 8. http://hdl.handle.net/10138/336063 (Accessed 8 Feb 2022).

Kalverla, P., Steeneveld, G.-J., Ronda, R., Holtslag, A.A.M., 2019. Evaluation of three mainstream numerical weather prediction models with observations from meteorological mast IJmuiden at the North Sea. Wind Energy 22, 34–48. https://doi.org/10.1002/we.2267.

Kim, Y., Sartelet, K., Raut, J.-C., Chazette, P., 2013. Evaluation of the weather research and forecast/urban model over greater Paris. Boundary-Layer Meteorol 149, 105–132. https://doi.org/10.1007/s10546-013-9838-6.

Kirthiga, S.M., Patel, N.R., 2018. Impact of updating land surface data on micrometeorological weather simulations from the WRF model. Atmósfera 31 (2), 165–183. https://doi.org/10.20937/atm.2018.31.02.05.

Klysik, K., Fortuniak, K., 1999. Temporal and spatial characteristics of the urban heat island of Lodz. Poland. Atmos. Environ. 33, 3885–3895. https://doi.org/10.1016/S1352-2310(99)00131-4.

Kollanus, V., Tiittanen, P., Lanki, T., 2021. Mortality risk related to heatwaves in Finland – factors affecting vulnerability. Environ. Res. 201, 111503 https://doi.org/10.1016/j.envres.2021.111503.

Landsberg, H.E., 1981. The Urban Climate. Academic Press, London.

Le Roy, B., Lemonsu, A., Schoetter, R., 2021. A statistical–dynamical downscaling methodology for the urban heat island applied to the EURO-CORDEX ensemble. Clim. Dyn. 56, 2487–2508. https://doi.org/10.1007/s00382-020-05600-z.

López-Espinoza, E.D., Zavala-Hidalgo, J., Mahmood, R., Gómez-Ramos, O., 2020. Assessing the impact of land use and land cover data representation on weather forecast quality: a case study in Central Mexico. Atmosphere 11 (11), 1242. https://doi.org/10.3390/atmos11111242.

MacLachlan, A., Biggs, E., Roberts, G., Boruff, B., 2021. Sustainable City planning: a data-driven approach for mitigating urban heat. Front. in Built Environ. 6, 200. https://doi.org/10.3389/fbuil.2020.519599.

Masson, V., 2000. A physically-based scheme for the urban energy budget in atmospheric models. Bound.-Layer Meteorol. 94, 357–397. https://doi.org/10.1023/A:1002463829265.

Masson, V., Le Moigne, P., Martin, E., Faroux, S., Alias, A., Alkama, R., Belamari, S., Barbu, A., Boone, A., Bouyssel, F., Brousseau, P., Brun, E., Calvet, J.-C., Carrer, D., Decharme, B., Delire, C., Donier, S., Essaouini, K., Gibelin, A.-L., Giordani, H., Habets, F., Jidane, M., Kerdraon, G., Kourzeneva, E., Lafaysse, M., Lafont, S., Lebeaupin Brossier, C., Lemonsu, A., Mahfouf, J.-F., Marguinaud, P., Mokhtari, M., Morin, S., Pigeon, G., Salgado, R., Seity, Y., Taillefer, F., Tanguy, G., Tulet, P., Vincendon, B., Vionnet, V., Voldoire, A., 2013. The SURFEXv7.2 land and ocean surface platform for coupled or offline simulation of earth surface variables and fluxes. Geosci. Model Dev. 6, 929–960. https://doi.org/10.5194/gmd-6-929-2013.

Mingarro, M., Lobo, J.M., 2023. European National Parks protect their surroundings but not everywhere: a study using land use/land cover dynamics derived from CORINE land cover data. Land Use Policy 124, 106434. https://doi.org/10.1016/j.landusepol.2022.106434.

Mirzaei, P.A., 2015. Recent challenges in modeling of urban heat island. Sustain. Cities Soc. 19, 200–206. https://doi.org/10.1016/j.scs.2015.04.001.

Moiret-Guigand, A., 2021. CORINE Land Cover 2018 and CORINE Land Cover Change 2012–2018 - Validation report. https://land.copernicus.eu/en/technical-library/clc-2018-and-clc-change-2012-2018-validation-report/@@download/file. Accessed 6 Sep 2023.

Nakata-Osaki, C.M., Souza, L.C.L., Rodrigues, D.S., 2018. THIS – tool for Heat Island simulation: a GIS extension model to calculate urban heat island intensity based on urban geometry. Comput. Environ. Urban Syst. 67, 157–168. https://doi.org/10.1016/j.compenvurbsys.2017.09.007.

Noilhan, J., Planton, S., 1989. A simple parameterization of land surface processes for meteorological models. Mon. Weather Rev. 117, 536–549, 10.115/1520-0493(1989)117<0536:ASPOLS>2.0.CO;2.

Oke, T.R., 1987. Boundary Layer Climates, 2nd edition. Routledge, London.

Oleson, K.W., Bonan, G.B., Feddema, J., Jackson, T., 2011. An examination of urban heat island characteristics in a global climate model. Int. J. Climatol. 31, 1848–1865. https://doi.org/10.1002/joc.2201.

Quah, A.K.L., Roth, M., 2012. Diurnal and weekly variation of anthropogenic heat emissions in a tropical city. Singapore. Atmos. Environ. 46, 92–103. https://doi.org/10.1016/j.atmosenv.2011.10.015.

Quitián-Hernández, L., Bolgiani, P., Santos-Muñoz, D., Sastre, M., Díaz-Fernández, J., González-Alemán, J.J., Farrán, J.I., Lopez, L., Valero, F., Martín, M.L., 2021. Analysis of the October 2014 subtropical cyclone using the WRF and the HARMONIE-AROME numerical models: assessment against observations. Atmos. Res. 260, 105697 https://doi.org/10.1016/j.atmosres.2021.105697.

Reinhart, V., Fonte Hoffmann, P., Bechtel, B., Rechid, D., Boehner, J., 2021. Comparison of ESA climate change initiative land cover to CORINE land cover over Eastern Europe and the Baltic States from a regional climate modeling perspective. Int. J. Appl. Earth Obs. Geoinf. 94, 102221 https://doi.org/10.1016/j.jag.2020.102221.

Roxon, J., Ulm, F.-J., Pellenq, R.J.-M., 2020. Urban heat island impact on state residential energy cost and CO2 emissions in the United States. Urban Clim. 31, 100546 https://doi.org/10.1016/j.uclim.2019.100546.

Rusu, A., Ursu, A., Stoleriu, C.C., Groza, O., Niacșu, L., Sfică, L., Minea, I., Stoleriu, O.M., 2020. Structural changes in the Romanian economy reflected through Corine land cover datasets. Remote Sens. 12, 1323. https://doi.org/10.3390/rs12081323.

Ruuhela, R., Jylhä, K., Lanki, T., Tiittanen, P., Matzarakis, A., 2017. Biometeorological assessment of mortality related to extreme temperatures in Helsinki region, Finland, 1972-2014. Int. J. Environ. Res. Public Health 14 (8), 944. https://doi.org/10.3390/ijerph14080944.

Ruuhela, R., Votsis, A., Kukkonen, J., Jylhä, K., Kankaanpää, S., Perrels, A., 2021. Temperature-related mortality in Helsinki compared to its surrounding region over two decades, with special emphasis on intensive heatwaves. Atmosphere 12 (1), 46. https://doi.org/10.3390/atmos12010046.

Saaroni, H., BenDor, E., Bitan, A., Potchter, O., 2000. Spatial distribution and microscale characteristics of the urban heat island in Tel Aviv, Israel. Landsc. Urban Plan. 48, 1–18. https://doi.org/10.1016/S0169-2046(99)00075-4.

Sailor, D.J., Georgescu, M., Milne, J.M., Hart, M.A., 2015. Development of a national anthropogenic heating database with an extrapolation for international cities. Atmos. Environ. 118, 7–18. https://doi.org/10.1016/j.atmosenv.2015.07.016.

Samsonov, T.E., Varentsov, M.I., 2020. Computation of City-descriptive parameters for high-resolution numerical weather prediction in Moscow megacity in the framework of the COSMO model. Russ. Meteorol. Hydrol. 45, 515–521. https://doi.org/10.3103/S1068373920070079.

Samuelsson, P., Kourzeneva, E., de Vries, J., and Viana Jiménez, S., 2020. HIRLAM experience with ECOCLIMAP second generation. ALADIN-HIRLAM newsletter 154–180. http://www.umr-cnrm.fr/aladin/IMG/pdf/nl14.pdf (accessed 17 March 2022).

Sandu, I., Beljaars, A., Bechtold, P., Mauritsen, T., Balsamo, G., 2013. Why is it so difficult to represent stably stratified conditions in numerical weather prediction (NWP) models? J. Adv. Model. Earth Syst. 5, 117–133. https://doi.org/10.1002/jame.20013.

Scott, A.A., Waugh, D.D., Zaitchik, B.F., 2018. Reduced urban Heat Island intensity under warmer conditions. Environ. Res. Lett. 13, 064003 https://doi.org/10.1088/1748-9326/aabd6c.

Sekula, P., Bokwa, A., Bochenek, B., Zimnoch, M., 2019. Prediction of air temperature in the polish Western Carpathian Mountains with the ALADIN-HIRLAM numerical weather prediction system. Atmosphere 10, 186. https://doi.org/10.3390/atmos10040186.

Serifi, A., Günther, T., Ban, N., 2021. Spatio-temporal downscaling of climate data using convolutional and error-predicting neural networks. Front. Clim. 3 https://doi.org/10.3389/fclim.2021.656479.

Sertel, E., Robock, A., Ormeci, C., 2010. Impacts of land cover data quality on regional climate simulations. Int. J. Climatol. 30, 1942–1953. https://doi.org/10.1002/joc.2036.

Shi, H., Xian, G., Auch, R., Gallo, K., Zhou, Q., 2021. Urban heat island and its regional impacts using remotely sensed thermal data—a review of recent developments and methodology. Land 10 (8), 867. https://doi.org/10.3390/land10080867.

Stewart, I.D., Oke, T.R., 2012. Local climate zones for urban temperature studies. Bull. Am. Meteorol. Soc. 93 (12), 1879–1900. https://doi.org/10.1175/BAMS-D-11-00019.1.

Suomi, J., Käyhkö, J., 2012. The impact of environmental factors on urban temperature variability in the coastal city of Turku, SW Fnland. Int. J. Climatol. 32, 451–463. https://doi.org/10.1002/joc.2277.

SYKE, 2021. CORINE maanpeite 2018. Suomen ympäristökeskus (Finnish Environment Institute). https://ckan.ymparisto.fi/dataset/corine-maanpeite-2018. (Accessed 14 September 2021).

SYKE, Aalto University, FMI, 2020. Climateguide.fi. Finnish Environment Institute, Aalto University, YTK, Finnish Meteorological Institute. https://ilmasto-opas.fi/en (accessed 8 Jun 2021).

Szymanowski, M., Kryza, M., 2009. GIS-based techniques for urban heat island spatialization. Clim. Res. 38, 171–187. https://doi.org/10.3354/cr00780.

Törmä, M., Markkanen, T., Hatunen, S., Härmä, P., Mattila, O.-P., Arslan, A.N., 2015. Assessment of land-cover data for land-surface modeling in regional climates studies. Boreal Environ. Res. 20, 243–260.

Turku, 2021. Turku map service. City of Turku. https://opaskartta.turku.fi. (Accessed 8 June 2021).

Voogt, J.A., Oke, T.R., 2003. Thermal remote sensing of urban climates. Remote Sens. Environ. 86, 370–384. https://doi.org/10.1016/S0034-4257(03)00079-8.

Waffle, A.D., Corry, R.C., Gillespie, T.J., Brown, R.D., 2017. Urban heat islands as agricultural opportunities: an innovative approach. Landsc. Urban Plan. 161, 103–114. https://doi.org/10.1016/j.landurbplan.2017.01.010.

Wilby, R.L., 2007. A review of climate change impacts on the built environment. Built Environ. 33 (1), 31–45. https://doi.org/10.2148/benv.33.1.31.